Cellulose (2018) 25:5791–5805
https://doi.org/10.1007/s10570-018-1984-z

ORIGINAL PAPER

Production of high lignin-containing and lignin-free cellulose nanocrystals from wood

Umesh P. Agarwal · Sally A. Ralph · Richard S. Reiner · Christopher G. Hunt · Carlos Baez · Rebecca Ibach · Kolby C. Hirth

Received: 16 April 2018 / Accepted: 8 August 2018 / Published online: 18 August 2018

Abstract A new method is described for producing high-lignin-containing and lignin-free cellulose nanocrystals from poplar wood (HLCNCs and LFCNCs, respectively). This was accomplished by first hydrothermally treating the poplar wood fibers at 170 °C for 45 min in a Parr reactor. For obtaining HLCNCs, the treated fibers were directly hydrolyzed by 64% sulfuric acid whereas for LFCNCs, the fibers were delignified prior to the acid hydrolysis. The CNCs thus produced were characterized using spectroscopy, microscopy, and diffraction techniques and compared with bleached kraft pulp-CNCs. The comparison indicated that while LFCNCs and pulp-CNCs had similar properties, the HLCNCs are expected to be superior for certain applications due to their hydrophobicity that was caused by presence of lignin nanoparticles. Lastly, results of the experiment where treatment temperature was varied during the hydrothermal treatment indicated that crystallinity of the CNCs produced from 200 °C treated poplar was higher compared to 170 °C treated substrate. This implied that CNCs from wood can be produced that have varying degree of crystallinity.

U. P. Agarwal (✉) · S. A. Ralph · R. S. Reiner · C. Baez
Fiber and Chemical Sciences Research, USDA FS, Forest Products Laboratory, 1 Gifford Pinchot Drive, Madison, WI 53726-2398, USA
e-mail: uagarwal@fs.fed.us

C. G. Hunt · R. Ibach
Forest Biopolymer Science and Engineering, USDA FS, Forest Products Laboratory, 1 Gifford Pinchot Drive, Madison, WI 53726-2398, USA

K. C. Hirth
Analytical Chemistry and Microscopy Laboratory, USDA FS, Forest Products Laboratory, 1 Gifford Pinchot Drive, Madison, WI 53726-2398, USA

Graphical abstract

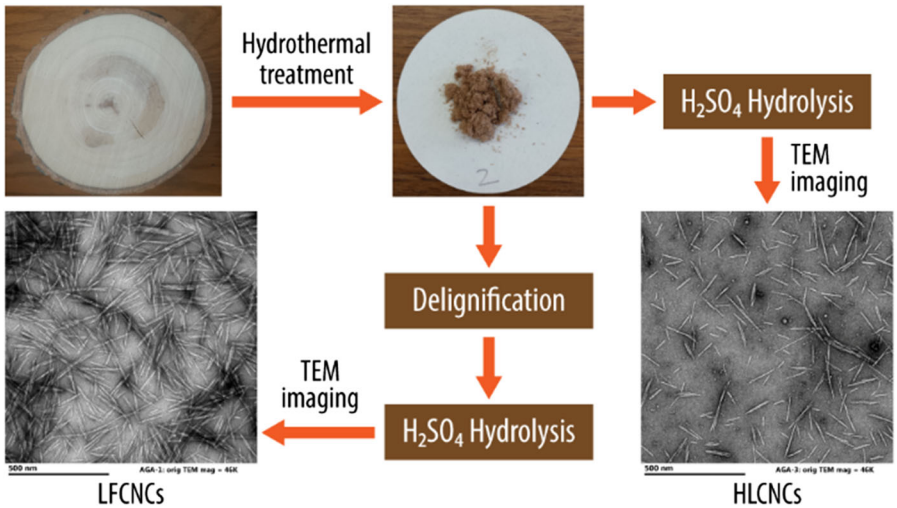

Keywords Wood · Hydrothermal treatment · Cellulose nanocrystals · Lignin-containing · Crystallinity

Introduction

Because of their unique characteristics (Habibi et al. 2010; Klemm et al. 2011; Moon et al. 2011; Sabo et al. 2016)—such as small size, high crystallinity, strong mechanical properties, surface charge density, density, and electrical and optical properties, CNCs are new exciting materials in the field of cellulose science and technology. The surface properties of the nanocelluloses can be further modified by functionalization. CNCs have been prepared from tunicate (Angles and Dufresne 2000), algae (Horikawa et al. 2018), cotton (Heux et al. 2000), bacterial cellulose (Grunert and Winter 2002), sugar beet (Azizi et al. 2004), wood (Abushammala et al. 2015), wood-pulp (Bian et al. 2017; Bondeson et al. 2006; Chen et al. 2015, 2016; Kvien et al. 2005), ramie (Lu et al. 2006), and wheat straw (Helbert et al. 1996). Their potential for applications is such that they are being presently produced commercially by a number of manufacturers (Mao et al. 2018). Some of the potential applications are in the fields of regenerative medicine (Domingues et al. 2014), optics (Iwamoto et al. 2005), composite films (Yu et al. 2013a, b), hydrogels (Yang et al. 2013), coatings (Poaty et al. 2014), pharmaceuticals and food packaging (Aulin et al. 2009; Goetz et al. 2009) as well as in the automotive sector (Dahlke et al. 1998). Although various cellulose substrates have been used for production of CNCs, most often, bleached kraft pulp has been the material of choice because it is cost-effectively produced by the pulp and paper industry, is readily available in large quantities, and consists of mostly cellulose (> 80%) (Agarwal et al. 2013).

In addition to lignin-free CNCs, nanocelluloses that contain lignin are desirable because this aromatic polymer is likely to impart desirable properties to the composites made from such CNCs and the adhesion between the CNCs and a hydrophobic polymer matrix can be improved (Grupper 2008; Gupta et al. 2017). For example, in the film, made using lignocellulosic nanofibrils, contribution of lignin to the formation, surface morphology, and physical behavior has been studied (Bian et al. 2018). Lignin imparted high hydrophobicity, high roughness, and high thermal stability.

As a biomass, wood is a renewable and biodegradable resource and can be produced from forests managed in a sustainable manner. Although wood contains pure cellulose microfibrils, according to recent findings (Agarwal et al. 2016), they are non-crystalline. However, this finding remains controversial in light of the generally believed alternative where wood cell wall microfibrils are considered to be semi-crystalline. It was reported that when untreated wood

was subjected to acid hydrolysis under conditions similar to that of kraft pulp CNCs production using sulfuric acid, no CNCs could be generated (Agarwal et al. 2016). Nevertheless, CNCs were produced from the same wood after it was heated to 170 °C in water and subsequently acid hydrolyzed (Agarwal et al. 2016). This suggested that the hydrothermal treatment was responsible for crystallization of the cellulose fibrils in wood (Agarwal et al. 2017a, 2018). Other reports of CNCs production from wood include use of ionic liquid whereby partially acetylated nanocrystals are generated (Abushammala et al. 2015), American Process Inc.'s AVAP (American Value Added Pulping) process (Nelson et al. 2016; Retsina and Nelson 2017), which produce CNCs with varying morphology and surface properties, and a Blue Goose process utilizing a catalytic conversion process (Olkowski and Laarveld 2013). The reader is referred to the respective references for further details on these processes as well as to a recent review on this topic (Mao et al. 2018).

The objective of the present research was to develop a method to directly produce CNCs (both lignin-containing and lignin-free) from woods. To meet that goal, wood fibers were treated hydrothermally to induce crystallization in cellulose fibrils (Agarwal et al. 2017a, 2018). Once the crystallization had occurred, the microfibrils were acid hydrolyzed to produce CNCs from wood.

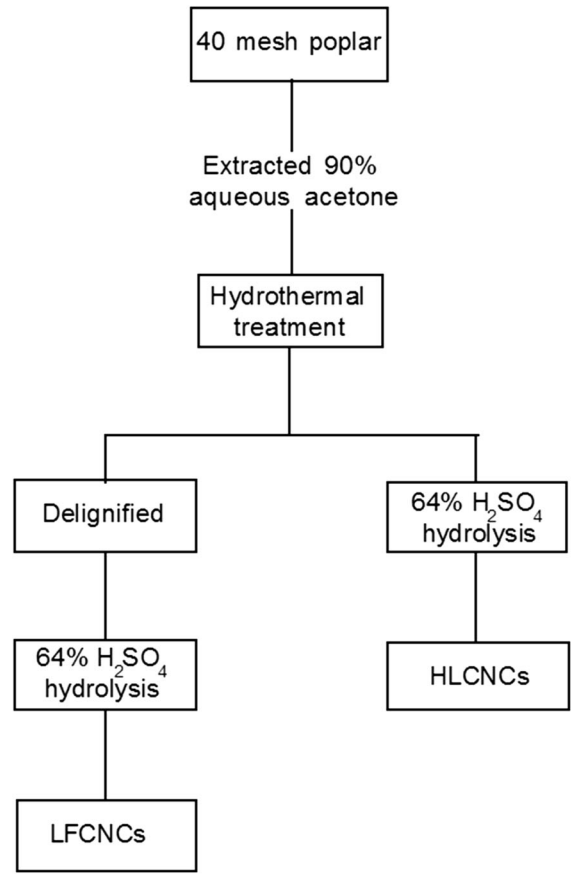

Scheme 1 Outline of production of CNCs from poplar; *LFCNCs* lignin free CNCs, *HLCNCs* high-lignin containing CNCs

Materials and methods

Chemicals

Monosodium phosphate and disodium phosphate (ACS grade) were purchased from Alfa Aesar (Tewksbury, MA). NaOH (AR grade) and sodium chlorite (technical grade) were obtained from Sigma-Aldrich (St. Louis, MO). Sulfuric acid (Certified ACS plus, 96% assay) and acetic acid (glacial) were from Fisher Scientific (Pittsburg, PA).

Hydrothermally treated poplar wood and CNCs production

The overall scheme of CNCs production from poplar (*Populus deltoids*) is shown in Scheme 1. The wood was Wiley milled to 40 mesh and extracted with acetone:water (9:1). Extracted wood meal (100 g) was mixed with 900 mL of 0.1 M pH 7.5 phosphate buffer, then heated (ramp time 45 min) in a 2 L horizontal Parr reactor with mixing to 170 °C and held at temperature for 45 min. After cooling quickly, the final pH was measured to be 5.2. The wood meal was filtered, washed well with reverse osmosis (RO) water and allowed to air dry (87.6 g, 87.6% yield from extracted wood). Treated wood meal (15 g) was mixed with 120 mL 64 wt% sulfuric acid under vacuum, then placed under a nitrogen atmosphere and stirred in a 45 °C water bath for 90 min. Then hydrolysis reaction was quenched by dilution with RO water to about 2 L. This suspension was neutralized using a 5 wt% NaOH solution. The suspension was diluted to 4.5 L and allowed to settle overnight. About 3.5 L of clear brown supernatant was decanted. The remaining suspension was transferred to a dialysis tube and

dialyzed against laboratory RO water for 1 week. The dialyzed suspension (900 mL) was treated with ultrasonic probe (20 kHz, 140 W) for 12 min. The suspension was then centrifuged for 15 min at 10,000 G and decanted. The solids were washed once by suspending again to 800 mL and centrifuging at 10,000*g* for 15 min. This decant was combined with the previous one and the total concentrated to about 42.9 g using a rotovap; a fraction was freeze dried to determine the solids content of HLCNCs at 4.50% (1.93 g total solids, 12.9% yield from heat treated wood). The solid lignin rich fraction from the centrifuge tubes were also freeze dried (3.23 g, 21.5% yield from hydrothermally treated wood).

Later on, similar hydrothermal treatments of poplar wood were also carried out at 100, 135, 170, and 200 °C using a Berghof reactor (Berghof Inc., Eningen, Germany) instead of a Parr reactor (Agarwal et al. 2018). In these treatments, the hold time at temperature was increased to 90 min from 45 min. Additionally, use of phosphate buffer was discontinued after it was found that the outcomes with and without buffer were similar and therefore, the use of buffer was inconsequential.

Delignification

A portion of the hydrothermal filter-cake was treated at 70 °C, over 9 h with 5 treatments of sodium chlorite and acetic acid, as per the method of Ahlgren and Goring (Ahlgren and Goring 1971). The residual, delignified treated wood was thoroughly washed with RO water but had some residual color and again was stored as the wet filter-cake. This delignified wood (holopulp) was used to produce LFCNCs by 64% H_2SO_4 hydrolysis using the method described above for the treated wood meal acid hydrolysis. For crystallinity determination by Raman spectroscopy, the holopulp was further treated with 4% NaOH at 70 °C for 4 h to remove any residual lignin and some of the hemicelluloses. Further, for Raman analysis, additional hydrothermally treated and untreated poplar wood samples were subjected to similar delignification and alkali treatments.

CNCs from bleached kraft pulp

Pulp-CNCs were produced from bleached softwood kraft pulp using the previously reported method (Agarwal et al. 2016; Reiner and Rudie 2013). The process used 64% sulfuric acid at 45 °C. Further details of the process can be found elsewhere (Agarwal et al. 2016; Reiner and Rudie 2013).

Transmission electron microscopy (TEM)

For TEM analysis of HLCNCs, LFCNCs, and pulp-CNCs, carbon grids (300 mesh) were floated on diluted sample droplets for $\sim$ 1 min prior to rinsing through stain (2% aqueous uranyl acetate) and blotting them dry. Samples were imaged using a Philips CM-100 TEM operated at 100 kV, spot 3, 200 µm condenser and 70 µm objective apertures. Images were captured in digital form directly on the microscope using Gatan Orius SC200-1 2 Mpixel CCD camera (Gatan, Inc., Pleasanton, CA). ImageJ (Program Image J) was used to manually measure the dimensions of the CNCs from their TEMs. At least 100 particles were measured for each type of CNCs and large clumps of particle that were suspected to be aggregates of drying were not measured. Similarly, small clumps or clusters were also excluded. In measuring CNC particles in ImageJ, if possible, straight line was chosen, otherwise, for long kinked specimens segmented option was chosen with 4–6 straight lines. Compared to CNC length measurements, widths were measured at higher magnification.

Using Microsoft Excel, on the width and length data of the CNCs, pairwise *t* tests at $p = 0.05$ were performed to determine if they were statistically different between the CNCs.

Chemical composition

Poplar, hydrothermally treated poplar, and CNC samples were analyzed for chemical composition. The amount of Klason lignin (TAPPI 1983) and carbohydrates (arabinan, galactan, glucan, xylan, and mannan) were determined (Davis 1998). Reproducibility for Klason lignin was 0.4%, and for the carbohydrate analysis, the standard deviation was $<$ 1% of assayed sugar (Davis 1998).

Sulfur analysis

The CNC samples were analyzed for sulfur content using an ICP-OES spectrometer Horiba (Edison, NJ) ULTIMA II with 12 L/min plasma gas, 0.2 L/min

sheath gas, 0.28 L/min nebulizer gas and a 20 µm/15 µm slit combination. Acquisition was done using 3 replicates in max mode with 0.5 s integration time. Calibration used a 7-point, linear external standardization with correlation coefficient > 0.999 for line 180.676 nm.

Thermogravimetric analysis (TGA)

The thermal properties were measured using a thermogravimetric analyzer, Perkin Elmer TGA 7 (PerkinElmer Inc., Waltham, MA). The TGA measurements were carried out in the temperature range 50–700 °C at a heating rate of 10 °C/min under N_2 atmosphere (20 mL/min).

Fourier transform infrared (FT-IR) spectroscopy

FT-IR spectra of the pulp-CNCs and hydrothermally treated poplar CNCs were obtained on a Spectrum Two system that was equipped with a universal attenuated-total-reflection (ATR) probe. The spectra were obtained in the range of 450–4000 cm^{-1} with a resolution of 4 cm^{-1}.

Recording Raman spectra and crystallinity estimation by Raman spectroscopy

Treated and untreated poplar, and the CNCs (pulp-CNCs and LFCNCs) were analyzed, in triplicate, with a Bruker (Billerica, MA) MultiRam equipped with a 1064-nm 1000 mW continuous wave (CW) diode pumped Nd:YAG laser. For each sample analysis, using 600 mW laser excitation, 1024 or 2048 scans were co-added. To reduce the fluorescence contribution in the Raman spectra, the hydrothermally treated wood samples were delignified and treated with alkali (see above). Sample pellets were made from $\sim$ 0.1 g of each sample. Bruker OPUS 7.2 software was used to process the spectral data which involved normalization, selection of a spectral region, background correction, and band integration. Background correction was performed using a 64 points OPUS "rubberband option". Cellulose crystallinity by Raman spectroscopy was estimated using two methods—380-Raman (Agarwal et al. 2010) and 93-Raman (Agarwal et al. 2018). Considering that 93-Raman method is very recent, for estimating the crystallinity, the following describes the manner in which the band intensities are calculated. Peak heights were calculated for bands at 1096 and 93 cm^{-1} by drawing a horizontal baseline under each of the bands. For the 1096 cm^{-1} band, this was accomplished by drawing a horizontal baseline from 944 cm^{-1} (minimum intensity wavenumber near 1096 cm^{-1} peak). Similarly, for the 93 cm^{-1} peak, a horizontal baseline from 70 cm^{-1} was drawn (minimum intensity wavenumber near the peak). Using the intensity data, ratios of peak heights (93 cm^{-1} to 1096 cm^{-1}) and ratios of 93 cm^{-1} peak areas to 1096 cm^{-1} peak heights were calculated. Further details on crystallinity estimation by 93-Raman method are provided by Agarwal et al. (Agarwal et al. 2018). For plotting purposes, the spectra were converted to ASCII format and exported to Excel.

X-ray diffraction and Segal-WAXS crystallinity calculation

Wide-angle X-ray diffraction (XRD) profiles were recorded at the Materials Research Science and Engineering Center, University of Wisconsin, Madison using a Bruker (Billerica, MA) D8 Discover diffractometer in reflection mode with 0.5 mm beam aperture and equipped with monochromatic CuKα (λ = 1.5418 Å) point source and a VÅNTEC-500 detector. The X-ray diffractometer beam aperture of 0.5 mm was used. In all cases, diffractograms were obtained on the same samples (in the pellet form) that were previously analyzed by FT-Raman spectroscopy. In case of HLCNCs for which no Raman spectrum could be obtained, for XRD, a pellet was made using 100 mg of the freeze-dried material. In XRD, both sides of the pellet were sampled and average values of the CrIs are reported. Segal-XRD CrI was calculated by measuring intensity at plane (200), I_{200}, and subtracting the amorphous contribution, I_{am}, at approximately $2\theta = 18°$ (Segal et al. 1959).

$$CrI = 100 * (I_{200} - I_{am})/I_{200} \quad (1)$$

This was done after a straight line was drawn between the lowest intensity points in the 2θ range of 7° and 37°. This method is similar to the (200) peak height ratio method (Park et al. 2010) although in the latter method, the background subtracted was based on a blank sample run. Previously, the authors have used this approach to determine Segal CrIs (Agarwal et al. 2013, 2016, 2017b).

Accessibility to water

To measure CNCs' accessibility to water (A), a previously reported procedure was used (Agarwal 2018; Foster et al. 2018). Briefly, the method is based on measuring increase of intensity of 1380 cm^{-1} Raman band in the spectrum of a CNCs sample after a complete OH-to-OD exchange has taken place (Agarwal et al. 2016). "A" is defined by Eq. 2 and for amorphous cellulose, was assumed to be 100%. In Eq. 2, for a sample, ΔI_{sample} is defined as % increase in the relative intensity of the 1380 cm^{-1} Raman band (relative to 1096 cm^{-1} band) when the OH-to-OD exchange is complete in the sample. Moreover, $\Delta I_{amorphous}$ is the % relative intensity increase for a similarly exchanged amorphous cellulose sample. Previously, Agarwal et al. (2016) have reported $\Delta I_{amorphous}$ value to be 154.3%.

$$A_{accessibility} = 100 * \left(\Delta I_{CNC} / \Delta I_{amorphous}\right) \quad (2)$$

Contact angle measurements

The static water contact angles of HLCNCs, LFCNCs, pulp-CNCs, and organosolv lignin were measured by the sessile drop method using a contact angle analyzer (Attension Theta, Biolin Scientific, Inc. Stockholm, Sweden). Samples, $\sim$ 33 mg each, were first pressed using a hydraulic press (Carver) at 14 MPa to make 8 mm diameter pellets and placed on the sample stage. A drop of distilled water of approximately 12 µL was automatically dispensed onto the surface of a pellet from a micro syringe. The software senses when the water drop contacts the sample surface and subsequently, records the contact angles as a function of time. Data analysis was performed using the OneAttension software provided with the instrument. The reported values are average of 10 consecutive readings.

Results and discussion

CNCs from hydrothermally treated poplar

Hydrothermal treatment causes significant changes in the composition and structure of wood. Although a complete knowledge is not yet available, it has been reported that in addition to changes in lignin and hemicelluloses, cellulose crystallinity increases (Agarwal et al. 2018; Assor et al. 2009; Inagaki et al. 2010; Yin et al. 2011). The mechanism of cellulose crystallization during the hydrothermal treatment is an area of ongoing research (Agarwal et al. 2018, Inagaki et al. 2010). Figure 1, from left to right, shows images of milled wood fibers (Fig. 1a), hydrothermally treated poplar (Fig. 1b), HLCNCs (Fig. 1c), and "solids from the centrifuge" fraction (Fig. 1d). Results of chemical analysis of these fractions, are reported in Table 1.

Of the four CNC samples in Table 1, the highest and lowest glucan content were in LFCNCs and the centrifuge fraction, respectively. This is in agreement with expectations because most of the crystalline cellulose is retained in the CNCs fraction (Table 1). Upon centrifugation, larger lignin particles settled to the bottom of the tubes (84% of the settled mass was lignin, Table 1), whereas the smaller lignin particles remained with the suspended CNCs. Comparing the hydrothermally treated and control poplar samples, the major compositional change was degradation of hemicelluloses resulting in higher glucan content compared to the control (Table 1).

Characterization of the CNCs

Typical TEMs of HLCNCs, LFCNCs, and pulp-CNCs are shown in Fig. 2. Lignin is distributed as small nanoparticles among the CNCs in HLCNCs (Fig. 2a), whereas, as expected, there are no such particles in the two lignin-free CNCs (Fig. 2b, c); and HLCNCs appear to be least aggregated (Fig. 2a–c). This is supported by the finding that freeze-dried HLCNCs had 29 times the surface area as freeze-dried pulp-CNCs (Wei et al. 2018). Based on image analysis of these CNCs, histograms of length and width distributions are shown in Fig. 2d–i. Moreover, the average size data with SD are reported in Table 2. From both the figure and table it can be seen that length increases through the series HLCNCs < LFCNCs < pulp-CNCs. Standard deviations (SD) also increase in the same order, but the length coefficient of variation (COV) values are comparable (Table 2) indicating similar length uniformity. CNCs' width increases in the same order as length, but not quite as quickly so the aspect ratio rises slightly through the series (Table 2). The SD and COV values for the width measurements

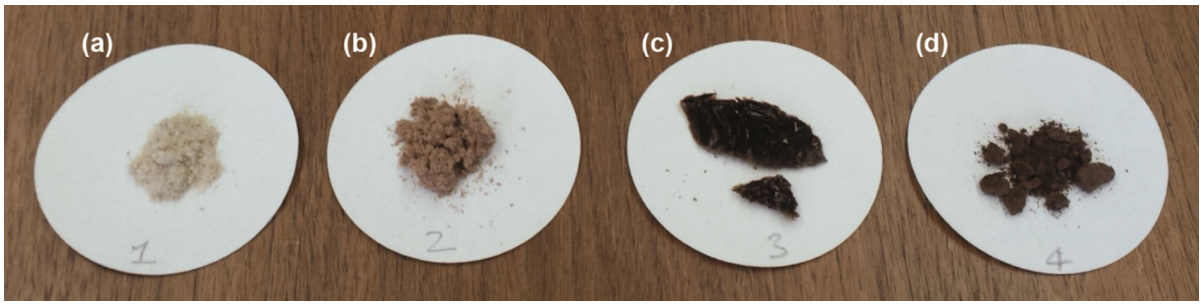

Fig. 1 Images of various samples derived from poplar wood; from left to right, **a** Wiley-milled, **b** hydrothermally treated, **c** HLCNCs, **d** lignin-rich fraction from the centrifuge

Table 1 Chemical analysis of various poplar fractions

Sample	Klason lignin (%)	Arabinan (%)	Galactan (%)	Glucan (%)	Xylan (%)	Mannan (%)	Tot. carbs. (%)	Tot. yield[a] (%)
Poplar wood	21.2	ND	0.72	47.73	13.02	2.89	64.36	85.0
Hydrothermally treated	22.6	ND	0.53	51.34	10.58	2.65	65.10	87.3
HLCNCs	30.6	ND	ND	56.44	1.01	ND	57.45	87.1
Centrifuge fraction	83.9	ND	ND	5.46	0.55	ND	6.01	89.7
LFCNCs	1.0	ND	ND	91.9	0.48	ND	92.4	92.4
Pulp-CNCs	1.0	ND	ND	85.01	3.64	ND	88.65	90.0

ND not detected

[a]Sum of total carbohydrates and Klason lignin

indicated that there were significant differences, especially between pulp-CNCs and HLCNCs. Using Excel, pairwise t tests at $p = 0.05$ showed all three CNCs had statistically different lengths and the 8 nm CNC width (HLCNCs) was different from the other two. The widths of LFCNCs and pulp-CNCs were not statistically different.

All measurements based on TEM images are limited by the potential biases of identifying edges, clumping, imaging artifacts, and sample selection, but compared to HLCNCs the lignin free CNCs appear to be more aggregated (Fig. 2a–c). The aggregation characteristic of the LFCNCs and pulp-CNCs imposes limitation on the image analysis approach because distinguishing between single versus aggregated CNCs becomes rather challenging. This explanation is further supported by the fact that compared to HLCNCs LFCNCs were, on average, 32% longer (Table 2), in principle, however, they should have been identical because the two CNCs were obtained from the same treated poplar. Further, pulp-CNCs were the longest ($\sim$ 50% longer, Table 2), and most aggregated of this series. This is nothing new because CNCs tendency to aggregate is well recognized (Brinkmann et al. 2015; Agarwal et al. 2012). For instance, based on AFM (atomic force microscopy) and TEM investigations it was reported that CNCs width by TEM was almost twice as large as AFM height (Brinkmann et al. 2015). This was thought to be due to CNCs that were laterally associated in the TEM images. By TEM, laterally associated CNCs are also likely to give longer length measurements.

Comparing the two lignin free CNCs, pulp-CNCs versus LFCNCs, the latter are less aggregated and more uniform in size (Fig. 2e vs. f and Fig. 2h vs. i; Table 2), which might be an advantage for functional applications that require good dispersion of CNCs.

Characterization by IR and Raman spectroscopy

For further physicochemical characterization and comparison of the 3 types of CNCs, ATR-IR (Fig. 3)

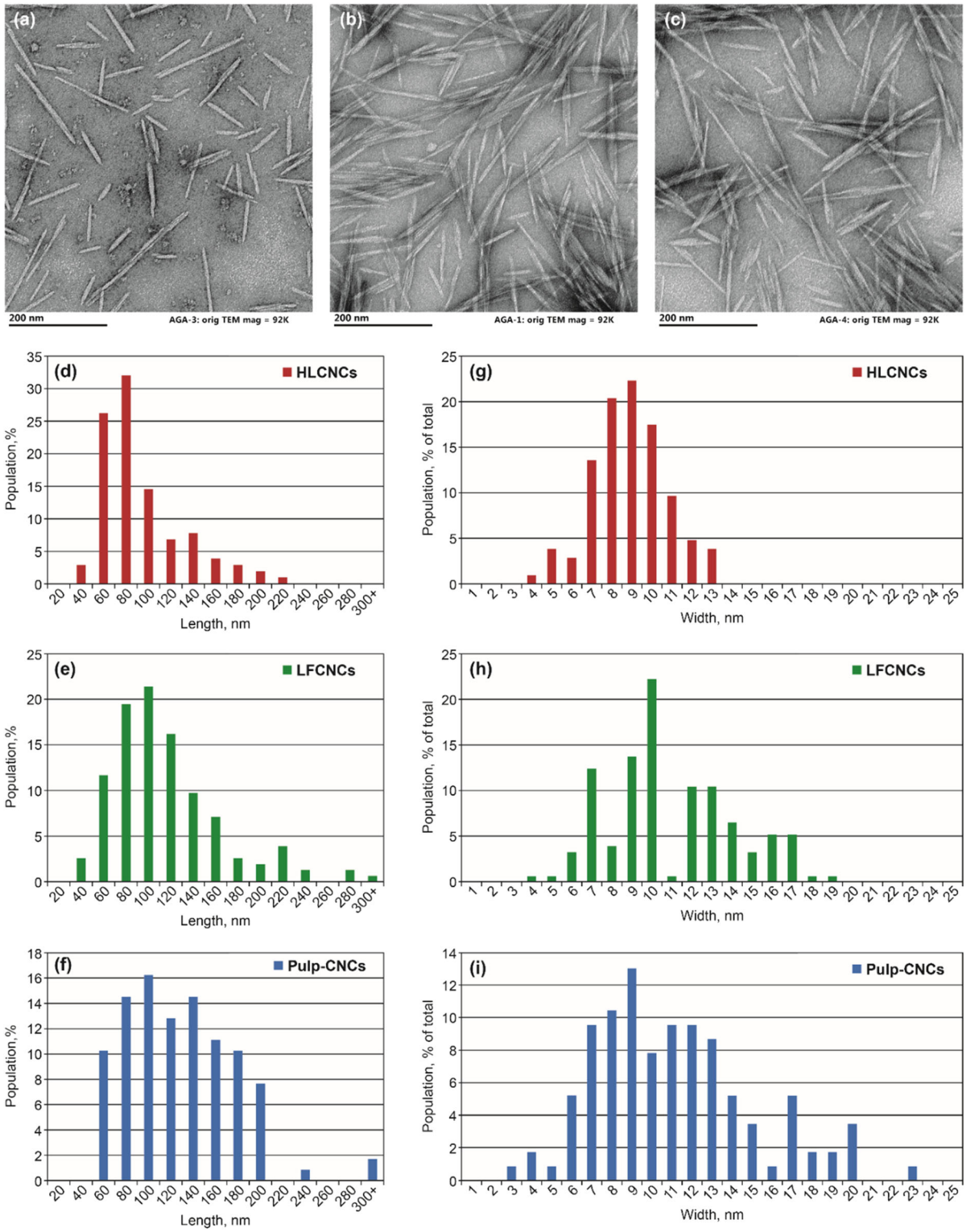

Fig. 2 TEM images of **a** HLCNCs, **b** LFCNCs, and **c** pulp-CNCs. In **a** lignin presence can be noted in terms of nano size spherical particles (2–22 nm). **d–i** Histograms of length and width distributions of the CNCs

Table 2 Comparison of wood- and pulp-CNCs

Characteristics	HLCNCs	LFCNCs	Pulp-CNCs
Average length (nm)	82 ± 36	108 ± 43	123 ± 58
Coefficient of variation	0.44	0.40	0.47
Average width (nm)	8.2 ± 1.8	10.2 ± 2.9	10.7 ± 3.9
Coefficient of variation	0.22	0.28	0.36
Aspect ratio	10.0	10.7	11.5
XRD crystallinity (%)	85.5	88.5	86.0
380-Raman crystallinity (%)	NA	54.0	54.5
93-Raman crystallinity (%)	NA	42.1	40.4
Accessibility to water (%)	NA	21.8	25.3
Sulfur content (wt%)	2.2	1.1	0.87
Degradation temperature, DTG[a] (°C)	390	328	322
Water contact angle (°)	52.5	36.0	26.1

NA not available, could not be estimated due to dark coloration of the CNCs

[a]Derivative thermogravimetric analysis; maximum in dTGA curve

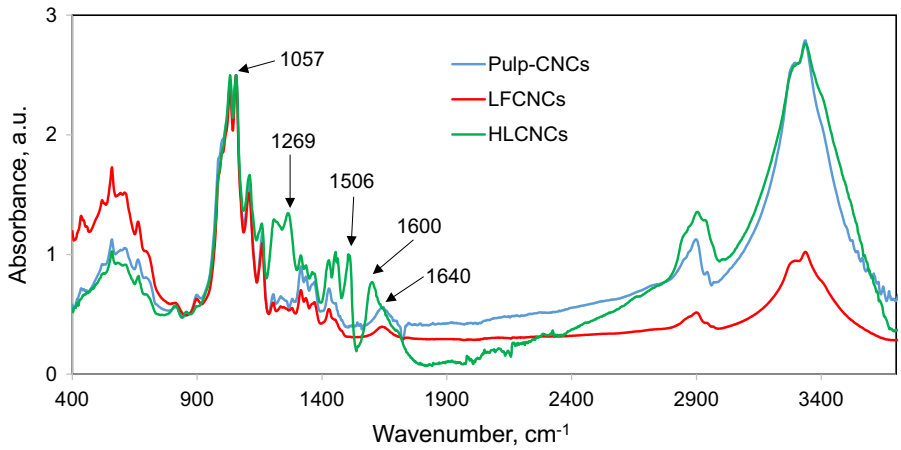

Fig. 3 1057 cm^{-1} normalized ATR-IR spectra of HLCNCs, LFCNCs, and pulp-CNCs

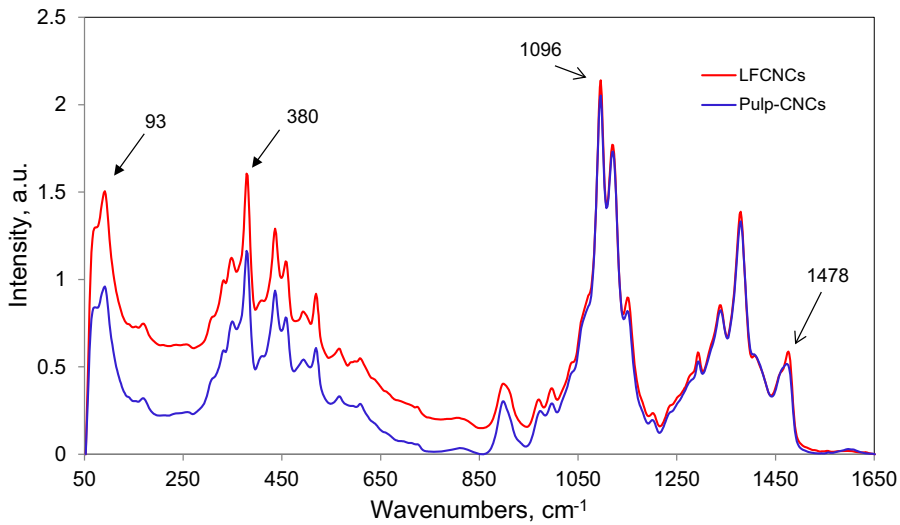

Fig. 4 FT-Raman spectra, 50–1650 cm^{-1} region, of LFCNCs and pulp-CNCs

and FT-Raman (Fig. 4) spectroscopies were used. The IR spectra in Fig. 3 were plotted after they were normalized to 1057 cm^{-1} band of cellulose. All three CNCs showed sharp features of cellulose (Abidi et al. 2010), some of which are annotated in Fig. 3. This indicated that cellulose's aggregated state in the CNCs was highly ordered and crystalline. Moreover, in the spectrum of HLCNCs, additional bands were present at 1269, 1506, and 1600 cm^{-1} indicating presence of lignin (Agarwal and Atalla 2010), which chemical analysis indicated was present at 30.6% (Table 1). As expected, these lignin IR bands were absent in the other lignin-free CNCs (Fig. 3). In the IR spectra of the samples, the band detected at $\sim$ 1640 cm^{-1} is due to water in the CNCs. The spectra also contained contributions of CH and OH stretching modes in the 2900 and 3300 cm^{-1} regions, respectively. Almost complete absence of hemicelluloses in the three CNCs (Table 1) was further supported by the IR spectra where no peak at $\sim$ 1740 cm^{-1} was detected (Fig. 3). This peak is associated with the stretching vibration of the carbonyl groups in hemicelluloses. However, deacetylation of hemicelluloses can also result in the reduction of this peak (Yin et al. 2011).

Raman spectrum of HLCNCs could not be obtained due to high fluorescence of lignin and therefore, LFCNCs and pulp-CNCs were compared (Fig. 4). Nevertheless, the ultrastructures of cellulose would be identical between HLCNCs and LFCNCs due to the fact that these LFCNCs were derived from the same treated poplar from which HLCNCs were obtained. Further, it has been reported that removal of lignin by acid chlorite method does not alter the ultrastructure of cellulose (Agarwal et al. 2014).

In Fig. 4, Raman spectra of LFCNCs and pulp-CNCs, reported in 50–1650 cm^{-1} region, were very similar and represented the ordered/crystalline state of cellulose (more later on crystallinity of the CNCs). In the spectra, some of the prominent peaks of cellulose have been identified. Particularly, bands at 93 and 380 cm^{-1} which have been used in the estimation of crystallinity of cellulose (Agarwal et al. 2010, 2013, 2018) were of comparable intensity in poplar and pulp derived CNCs. As was the case in IR (i.e., no evidence for presence of hemis or lignin), for LFCNCs and pulp-CNCs, no Raman contributions from lignin or hemicelluloses were detected (Agarwal and Ralph 1997).

Crystallinity by XRD and Raman spectroscopy

Crystallinity (CrI) was determined by XRD and Raman spectroscopy. The Raman spectra (Fig. 4) and the diffractograms of the CNCs (Fig. 5) were used to estimate the CrIs. Both, the XRD patterns and Raman spectra, indicated that cellulose's aggregated state in the CNCs was Iβ (Agarwal et al. 2017a, b; French and Santiago Cintrón 2013). Moreover, it has been reported that upon hydrothermal treatment crystallinity of wood-cellulose increases (Agarwal et al. 2018; Inagaki et al. 2010; Silveira et al. 2016).

Estimation of CrI by Raman spectroscopy were based on two methods – 380-Raman (Agarwal et al. 2010) and 93-Raman (Agarwal et al. 2018). The XRD and Raman spectroscopy based CrIs are reported in Table 2. Because no fluorescence free Raman spectra could be obtained for HLCNCs the 93-Raman CrI could not be calculated for this sample. However, 380-Raman estimated cellulose crystallinity is not influenced by presence of syringyl lignin (likely to be present in poplar Klason lignin) because prior to estimating cellulose crystallinity the lignin is removed (Agarwal et al. 2013; 2014). Therefore, latter's cellulose Raman CrIs can be assumed to be very similar to that of LFCNCs. In Table 2, 380-Raman CrI data showed that CrIs of pulp-CNCs and LFCNCs were similar whereas based on XRD and 93-Raman data LFCNCs were slightly more crystalline.

Accessibility to water

The accessibility to water (Agarwal 2018; Foster et al. 2018) "*A*" is reported in Table 2. By accessibility to water of a CNC what is meant is the amount of non-

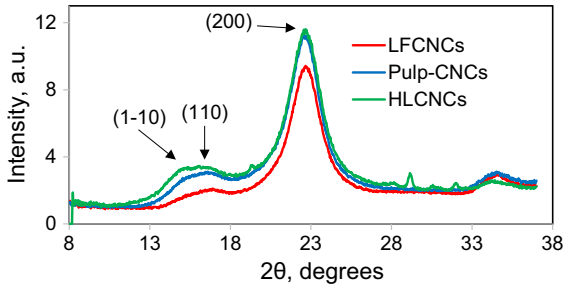

Fig. 5 XRD patterns of HLCNCs, LFCNCs, and pulp-CNCs. In case of HLCNCs, minor contamination peaks appeared at $\sim$ 19.5, 28, 30–31, and 32.5 degrees and are likely to be due to Na_2SO_4

crystalline phase (including the crystal surface) in CNCs that can be accessed by water. The data indicated that compared to pulp-CNCs *A* of the LFCNCs was slightly lower. This is likely to be due to slightly higher 93-Raman CrI of wood-CNCs compared to pulp-CNCs (Table 2) which implies that, in the former, there are fewer regions in the ultra-structure of cellulose that can be accessed by water molecules. In certain applications of CNCs, low accessibility to water is a desirable property (e.g., gas percolation in membranes). In this context, it should be noted that compared to 380-Raman and XRD, 93-Raman crystallinity estimation method is more reliable because contributions from non-crystalline phases of cellulose are avoided (Agarwal et al. 2018).

Extent of sulfation

The sulfur present in HLCNCs was 2 and 2.5 times the amount present in, respectively, LFCNCs and pulp-CNCs (Table 2). Although the overall sulfur amount was higher in HLCNCs, it is not known which of the two components (cellulose and lignin) is responsible for it. Nevertheless, compared to LFCNCs which are lignin free and derived from same treated poplar as HLCNCs, the two times higher sulfur content in the latter is likely to be due to the lignin fraction. Existence of higher amount of anionic sulfate groups implies greater surface charge in the HLCNCs which usually indicates better dispersibility.

Thermal properties by TGA

For composite applications of CNCs, their thermal stability and degradation characteristics are important considerations (Yu et al. 2013a, b; Petersson et al. 2007). The thermogravimetric (TG) and derivative thermogravimetric (DTG) analyses were used to measure weight loss and rate of change of weight loss f(dW/dT) and determine thermal stability of the CNC samples. TG and DTG curves of HLCNCs, LFCNCs and pulp-CNCs are shown in Fig. 6. The thermal transformation of the CNCs occur in the following steps: (1) water evaporation and decomposition of low molecular weight polysaccharides; (2) decomposition of cellulose and lignin (if present); and (3) degradation of remaining materials. Comparing the water evaporation region between pulp-CNCs and wood-CNCs (Fig. 6), the former showed some mass loss which is likely to be due to moisture content differences between the two samples. This is supported by pulp-CNCs being somewhat less crystalline compared to LFCNCs (93-Raman data, Table 2), the sample seems to retain more water. The onset temperature (the temperature at which the weight loss begins) for HLCNCs was approximately 30 °C higher compared to the other CNCs (337 vs. 300 °C, Fig. 6). Similarly, the temperature of maximum degradation rate of sample HLCNCs was ~ 60 °C higher than of pulp-CNCs and LFCNCs (Table 2). Based on prior studies, it is known that sulfated CNCs thermally degraded more easily than non-sulfated CNCs (Lin and Dufresne 2014). However, because all three types of the CNCs investigated in this work were sulfated and the sulfation level of HLCNCs was higher, the higher thermal stability of this CNC is likely due to presence of lignin (Bian et al. 2017; Carrillo et al. 2018). Lignin, which is thermally more stable than cellulose, is known to play this role—untreated softwood whose lignin content is ~ 28% has higher thermal stability compared to delignified-wood (holopulp or holocellulose) (Carrillo et al. 2018). The other two CNCs, although sulfated (Table 2), contained no lignin and showed relatively poor thermal stability (Fig. 6). At 500 °C, about 64% of HLCNC mass was lost. This compares to 79 and 70% degradation, respectively, of LFCNCs and pulp-CNCs at this temperature. Therefore, the CNC samples can be differentiated based on their thermal stabilities which are important if CNCs are used in high temperature processes such as composite extrusion.

Hydrophobicity (water contact angle)

Considering that a significant amount (31%, Table 1) of lignin is present in HLCNCs, one expects these CNCs to be more hydrophobic compared to the lignin free CNCs. The water contact angle for the CNCs are reported in Table 2. Compared to pulp-CNCs, the contact angle of HLCNCs was two times higher (Table 2) and is caused by the hydrophobic nature of the high lignin CNCs. LFCNCs showed the intermediate value of 36 (Table 2) but was significantly higher compared to pulp-CNCs. As expected, these values were all lower compared to water contact angle of organosolv lignin which gave a value of 102.8. Results, similar to HLCNCs, on lignin containing

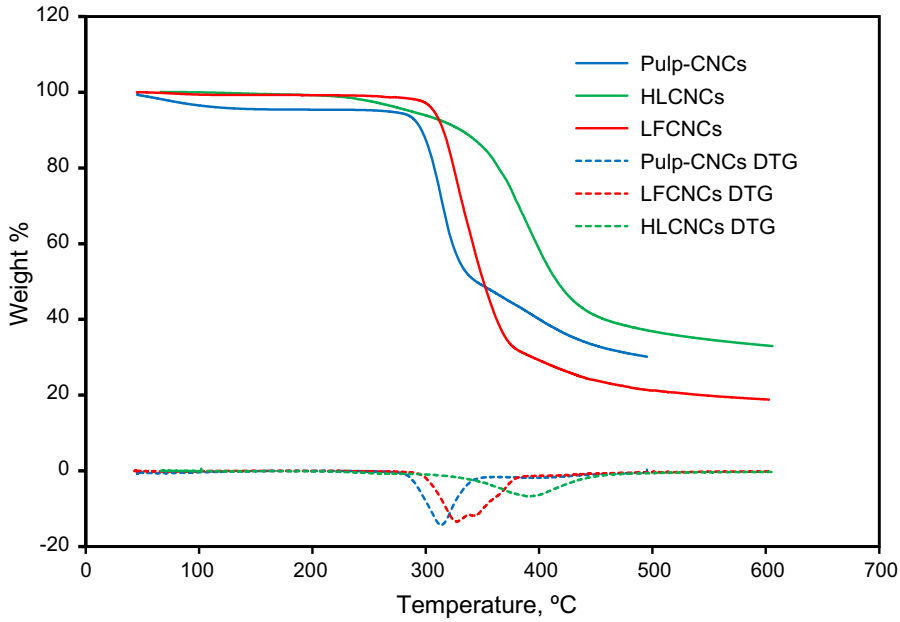

Fig. 6 Thermograms (TG) and differential thermograms (DTG) of the wood- and pulp-CNCs

nanocellulose films have been previously reported (Bian et al. 2018). Therefore, for composite applications where synthetic hydrophobic/non-polar polymers are used as a matrix and CNCs as a reinforcement component, improved interfacial interactions with the matrix are expected. Indeed, in a recent report that compounded HLCNCs with poly(lactic acid), improved composite properties were obtained (Wei et al. 2018) that were better than that of pulp-CNCs/poly(lactic acid) composite.

Crystallinity control

The crystallinity measurement of the poplar samples that were hydrothermally treated at different temperatures indicated that CrI depended upon the temperature of the treatment (Agarwal et al. 2018). As an example, for the 170 and 200 °C treated substrates, estimated CrIs based on various methods (93-Raman, 380-Raman, and Segal-WAXS) are reported in Table 3. Based on 93-Raman method, LFCNCs produced from 200 °C treated substrate was 32.8% more crystalline (13.8% increase in absolute CrI) compared to the materials treated at 170 °C (Table 3). Although the absolute percentages of the CrI increases were lower, similar results were also obtained when the crystallinity was estimated by 380-Raman and Segal-WAXS (Table 3). This observation suggested that the crystallinity of the wood-CNCs can be tuned to some degree. Additional investigations are needed to further develop this topic.

Advantages of wood-CNCs

In the context of commercialization of CNCs for various applications, both lignin free (LFCNCs) and high-lignin containing CNCs (HLCNCs) can be produced directly from wood. However, considering that, worldwide, wood-pulp industry is well established and economical, there has to be significant

Table 3 Percentage crystallinities of treated poplar and CNCs

Sample	93-Raman	380-Raman	Segal-WAXS
170 °C treated poplar	30.4	57.2	84.5
200 °C treated poplar	41.3	67.1	90.0
LFCNCs from 170 °C sample	42.1	54.0	88.5
LFCNCs from 200 °C sample	55.9	62.0	91.5
Difference in CNCs crystallinity, 200 versus 170 °C	13.8	8.0	3.0

advantages of the wood-CNCs that are beyond what is offered by pulp-CNCs. Although small beneficial differences exist between LFCNCs and pulp-CNCs (e.g., crystallinity control), the main advantage is the high lignin content HLCNCs (31% in the present case, Table 1) and the manner in which lignin is dispersed between the nanocrystals of cellulose (Fig. 2a). This results in less aggregated CNCs that are hydrophobic in nature. Although a few reports of lignin containing CNCs exist in the literature (Bian et al. 2017; Retsina and Nelson 2017), overall, these CNCs are inferior when CNC-width, yield, and % lignin content are considered. In one case (Bian et al. 2017), two types of CNCs with lignin content 4.6 and 18% were reported. For these, the yields for higher- and lower-lignin CNCs were 2.1 and 6.0%, respectively (Bian et al. 2017). In another case (Retsina and Nelson 2017), where lignin-coated CNCs were produced, the sulfonated-lignin was precipitated only on the surface of the CNCs and in amounts about 1% or less (Retsina and Nelson 2017). In our case, using HLCNCs in composite-applications where better interactions with the polymer matrix are desired, the initial results seem to be encouraging (Wei et al. 2018). The reported HLCNCs yield of 12.9% in the present study is likely to be further improved after the experimental conditions of HLCNCs production are optimized. Such conditions have to do mostly with the acid hydrolysis portion of the production process. The variables that need optimization are acid concentration, duration of hydrolysis, and temperature of hydrolysis. Additional work is expected to result in further progress.

Conclusions

HLCNCs and LFCNCs from wood were prepared by hydrothermal treatment followed by 64% sulfuric acid hydrolysis. In HLCNCs, a significant amount of originally present lignin was retained whereas in LFCNCs lignin was completely removed prior to the acid hydrolysis. In HLCNCs, lignin was found to be distributed in the nano form and imparted high thermal stability and hydrophobicity. The CrI of CNCs was found to increase with increasing hydrothermal treatment temperature. Compared to LFCNCs and pulp-CNCs, HLCNCs are suited for making superior polymeric nanocomposites wherein they are likely to provide increased reinforcing effect.

Acknowledgments The authors thank Ms. Debby Sherman (DSimaging, LLC) for obtaining the TEMs of CNCs. Also, Fred Matt of Analytical Chemistry and Microscopy Laboratory is acknowledged for the chemical analyses of the samples. The authors gratefully acknowledge use of X-ray facilities and instrumentation supported by NSF through the University of Wisconsin Materials Research Science and Engineering Center (DMR-1121288).

Author Contributions The manuscript was written through contributions of all authors. All authors have given approval to the final version of the manuscript.

References

Abidi N, Cabrales L, Hequet E (2010) Fourier transform infrared spectroscopic approach to the study of the secondary cell wall development in cotton fiber. Cellulose 17:309–320

Abushammala H, Krossing I, Laborie MP (2015) Ionic liquid-mediated technology to produce cellulose nanocrystals directly from wood. Carbohyd Polym 134:609–616

Agarwal UP (2018) Raman spectroscopy in the analysis of cellulose nanomaterials. In: Agarwal UP, Atalla RH, Isogai A (eds) Nanocelluloses: their preparation, properties, and applications, ACS symposium series, chapter 4. American Chemical Society, Washington **(in press)**

Agarwal UP, Atalla RH (2010) Vibrational spectroscopy. In: Heitner C, Dimmel D, Schmidt J (eds) Lignin and lignans: advances in chemistry, chapter 4. CRC Press, Boca Raton, pp 103–135

Agarwal UP, Ralph SA (1997) FT-Raman spectroscopy of wood: identifying contributions of lignin and carbohydrate polymers in the spectrum of black spruce (*Picea mariana*). Appl Spectrosc 51:1648–1655

Agarwal UP, Reiner RS, Ralph SA (2010) Cellulose I crystallinity determination using FT–Raman spectroscopy: univariate and multivariate methods. Cellulose 17:721–733

Agarwal UP, Sabo R, Reiner RS, Clemons CM, Rudie AW (2012) Spatially resolved characterization of cellulose nanocrystal-polypropylene composite by confocal Raman microscopy. Appl Spectrosc 66:750–756

Agarwal UP, Reiner RS, Ralph SA (2013) Estimation of cellulose crystallinity of lignocelluloses using near-IR FT–Raman spectroscopy and comparison of the Raman and Segal-WAXS methods. J Agric Food Chem 61:103–113

Agarwal UP, Ralph SA, Reiner RS, Moore RK, Baez C (2014) Impacts of fiber orientation and milling on observed crystallinity in jack pine. Wood Sci Technol 48:1213–1227

Agarwal UP, Ralph SA, Reiner RS, Baez C (2016) Probing crystallinity of never-dried wood cellulose with Raman spectroscopy. Cellulose 23:125–144

Agarwal UP, Ralph SA, Reiner RS, Baez C (2017a) Production of cellulose nanocrystals from raw wood via hydrothermal treatment. US patent application 20170260692. https://

patents.google.com/patent/US20170260692A1/en?oq=15455211
Agarwal UP, Ralph SA, Baez C, Reiner RS, Verrill SP (2017b) Effect of sample moisture content on XRD-estimated cellulose crystallinity index and crystallite size. Cellulose 24:1971–1984
Agarwal UP, Ralph SA, Reiner RS, Baez C (2018) New cellulose crystallinity estimation method that differentiates between organized and crystalline phases. Carbohyd Polym 190:260–270
Ahlgren PA, Goring DAI (1971) Removal of wood components during chlorite delignification of black spruce. Can J Chem 49:1272–1275
Angles MN, Dufresne A (2000) Plasticized starch/tunicin whiskers nanocomposites. 1. Structural analysis. Macromolecules 33:8344–8353
Assor C, Placet V, Chabbert B, Habrant A, Lapierre C, Pollet B, Perre P (2009) Concomitant changes in viscoelastic properties and amorphous polymers during the hydrothermal treatment of hardwood and softwood. J Agric Food Chem 57:6830–6837
Aulin C, Ahola S, Josefsson P, Nishino T, Hirose Y, Österberg M, Wågberg L (2009) Nanoscale cellulose films with different crystallinities and mesostructures—their surface properties and interaction with water. Langmuir 25:7675–7685
Azizi MASA, Alloin F, Paillet M, Dufresne A (2004) Tangling effect in fibrillated cellulose reinforced nanocomposites. Macromolecules 37:4313–4316
Bian H, Chen L, Dai H, Zhu JY (2017) Integrated production of lignin containing cellulose nanocrystals (LCNC) and nanofibrils (LCNF) using an easily recyclable di-carboxylic acid. Carbohyd Polym 167:167–176
Bian H, Gao Y, Wang R, Liu Z, Wu W, Dai H (2018) Contribution of lignin to the surface structure and physical performance of cellulose nanofibrils film. Cellulose. https://doi.org/10.1007/s10570-018-1658-x
Bondeson D, Mathew AP, Oksman K (2006) Optimization of the isolation of nanocrystals from microcrystalline cellulose by acid hydrolysis. Cellulose 13:171–180
Brinkmann A, Chen M, Couillard M, Jakubek ZJ, Leng T, Johnston LJ (2015) Correlating cellulose nanocrystal particle size and surface area. Langmuir 32:6105–6114
Carrillo I, Mendonça RT, Ago M, Rojas OJ (2018) Comparative study of cellulosic components isolated from different Eucalyptus species. Cellulose. https://doi.org/10.1007/s10570-018-1653-2
Chen L, Wang Q, Hirth K, Baez C, Agarwal UP, Zhu JY (2015) Tailoring the yield and characteristics of wood cellulose nanocrystals (CNC) using concentrated acid hydrolysis. Cellulose 22:1753–1762
Chen L, Zhu JY, Baez C, Kitin P, Elder T (2016) Highly thermal-stable and functional cellulose nanocrystals and nanofibrils produced using fully recyclable organic acids. Green Chem 18:3835–3843
Dahlke B, Larbig H, Scherzer HD, Poltrock R (1998) Natural fiber reinforced foams based on renewable resources for automotive interior applications. J Cell Plast 34:361–379
Davis MW (1998) A rapid method for compositional carbohydrate analysis of lignocellulosics by high pH anion-exchange chromatography with pulse amperometric detection (HPAE/PAD). J Wood Chem Technol 18:235–252
Domingues R, Gomes ME, Reis RL (2014) The potential of cellulose nanocrystals in tissue engineering strategies. Biomacromolecules 15:2327–2346
Foster EJ, Moon RJ, Agarwal UP, Bortner MJ, Bras J, Camarero-Espinosa S, Chan KJ, Clift MJD, Cranston ED, Eichhorn SJ, Fox DM, Hamad WY, Heux L, Jean B, Korey M, Nieh W, Ong KJ, Reid MS, Renneckar S, Roberts R, Shatkin JA, Simonsen J, Stinson-Bagby K, Wanasekara N, Youngblood J (2018) Current characterization methods for cellulose nanomaterials. Chem Soc Rev 47:2609–2679
French AD, Santiago Cintrón M (2013) Cellulose polymorphy, crystallite size, and the Segal crystallinity index. Cellulose 20:583–588
Goetz L, Mathew A, Oksman K, Gatenholm P, Ragauskas AJ (2009) A novel nanocomposite film prepared from cross-linked cellulosic whiskers. Carbohyd Polym 75:85–89
Grunert M, Winter WT (2002) Nanocomposites of cellulose acetate butyrate reinforced with cellulose nanocrystals. J Polym Environ 10:27–30
Grupper N (2008) Application of lignin as natural adhesion promoter in cotton fibre-reinforced poly(lactic acid) (PLA) composites. J Mater Sci 43:5222–5229
Gupta A, Simmons W, Schueneman GT, Hylton D, Mintz EA (2017) Rheological and thermo-mechanical properties of poly(lactic acid)/lignin-coated cellulose nanocrystal composites. ACS Sustain Chem Eng 5:1711–1720
Habibi Y, Lucia LA, Rojas OJ (2010) Cellulose nanocrystals: chemistry, self-assembly, and applications. Chem Rev 110:3479–3500
Helbert W, Cavaille JY, Dufresne A (1996) Thermoplastic nanocomposites filled with wheat straw cellulose whiskers. Part I: processing and mechanical behavior. Polym Compos 17:604–611
Heux L, Chauve G, Bonini C (2000) Nonflocculating and chiral nematic self-ordering of cellulose microcrystals suspensions in nonpolar solvents. Langmuir 16:8210–8212
Horikawa Y, Shimizu M, Saito T, Isogai A, Imai T, Sugiyama J (2018) Influence of drying of chara cellulose on length/length distribution of microfibrils after acid hydrolysis. Int J Biol Macromol 109:569–575
Inagaki T, Siesler HW, Mitsui K, Tsuchikawa S (2010) Difference of the crystal structure of cellulose in wood after hydrothermal and aging degradation: a NIR spectroscopy and XRD study. Biomacromolecules 11:2300–2305
Iwamoto S, Nakagaito AN, Yano H, Nogi M (2005) Optically transparent composites reinforced with plant fiber-based nanofibers. Appl Phys A 81:1109–1112
Klemm D, Kramer F, Moritz S, Lindstrom T, Ankerfors M, Gray D, Dorris A (2011) Nanocelluloses: a new family of nature-based materials. Angew Chem Int Ed 50:5438–5466
Kvien I, Tanem BS, Oksman K (2005) Characterization of cellulose whiskers and their nanocomposites by atomic force and electron microscopy. Biomacromolecules 6:3160–3165
Lin N, Dufresne A (2014) Surface chemistry, morphological analysis and properties of cellulose nanocrystals with gradiented sulfation degrees. Nanoscale 6:5384–5393
Lu Y, Weng L, Cao X (2006) Morphological thermal and mechanical properties of ramie crystallites-reinforced

plasticized starch biocomposites. Carbohyd Polym 63:198–204

Mao J, Abushammala H, Brown N, Laborie MP (2018) Comparative assessment of methods for producing cellulose I nanocrystals from cellulosic sources. In: Agarwal UP, Atalla RH, Isogai A (eds) Nanocelluloses: their preparation, properties, and applications, ACS symposium series, chapter 2. American Chemical Society, Washington **(in press)**

Moon RJ, Martini A, Nairn J, Simonsen J, Youngblood J (2011) Cellulose nanomaterials review: structure, properties and nanocomposites. Chem Soc Rev 40:3941–3994

Nelson K, Retsina T, Iakovlev M, van Heiningen A, Deng Y, Shatkin JA, Mulyadi A (2016) American process: production of low cost nanocellulose for renewable, advanced materials applications. In: Madsen L, Svedberg E (eds) Materials research for manufacturing. Springer series in materials science, vol 224. Springer, Cham

Olkowski AA, Laarveld B (2013) Catalytic biomass conversion. http://www.google.com/patents/WO2013000074A1?cl=en

Park S, Baker JO, Himmel ME, Parilla PA, Johnson DK (2010) Cellulose crystallinity index: measurement techniques and their impact on interpreting cellulase performance. Biotechnol Biofuels 3:10

Petersson L, Kvien I, Oksman K (2007) Structure and thermal properties of poly(lactic acid)/cellulose whiskers nanocomposite materials. Compos Sci Technol 67:2535–2544

Poaty B, Vardanyan V, Wilczak L, Chauve G, Riedl B (2014) Modification of cellulose nanocrystals as reinforcement derivatives for wood coatings. Prog Org Coat 77:813–820

Reiner RS, Rudie AW (2013) Process scale-up of cellulose nanocrystal production to 25 kg per batch at the Forest Products Laboratory. In: Postek MT, Moon RJ, Rudie AJ, Bilodeau MA (eds) Production and applications of cellulose nanomaterials. TAPPI Press, Atlanta, pp 21–24

Retsina T, Nelson K (2017) Nanocellulose compositions and processes to produce same. US patent application US20170190800. http://www.google.com/patents/US20170190800

Sabo RC, Yermakov A, Law CT, Elhajjar R (2016) Nanocellulose-enabled electronics, energy harvesting devices, smart materials and sensors: a review. J Renew Mater 4:297–312

Segal L, Creely JJ, Martin AE, Conrad CM (1959) An empirical method for estimating the degree of crystallinity of native cellulose using the x-ray diffractometer. Text Res J 29:786–794

Silveira RL, Stoyanov SR, Kovalenko A, Skaf MS (2016) Cellulose aggregation under hydrothermal pretreatment conditions. Biomacromolecules 17:2582–2590

TAPPI Test Method (1983) Acid insoluble lignin in wood and pulp; official test method T-222 (Om). TAPPI, Atlanta

Wei L, Agarwal UP, Matuana L, Sabo RC, Stark NM (2018) Performance of high lignin content cellulose nanocrystals in poly (lactic acid). Polymer 135:305–313

Program ImageJ. https://imagej.nih.gov/ij/

Yang J, Han C, Duan J, Xu F, Sun R (2013) Mechanical and viscoelastic properties of cellulose nanocrystals reinforced poly(ethylene glycol) nanocomposite hydrogels. ACS Appl Mater Interfaces 5:3199–3207

Yin Y, Berglund L, Salmen L (2011) Effect of steam treatment on the properties of wood cell walls. Biomacromolecules 12:194–202

Yu H, Qin Z, Liang B, Liu N, Zhou Z, Chen L (2013a) Facile extraction of thermally stable cellulose nanocrystals with a high yield of 93% through hydrochloric acid hydrolysis under hydrothermal conditions. J Mater Chem A 1:3938–3944

Yu H, Qin Z, Liu L, Yang X, Zhou Y, Yao J (2013b) Comparison of the reinforcing effects for cellulose nanocrystals obtained by sulfuric and hydrochloric acid hydrolysis on the mechanical and thermal properties of bacterial polyester. Compos Sci Technol 87:22–28